Transp Porous Med (2013) 96:203–220
DOI 10.1007/s11242-012-0084-z

Wormhole Propagation Behavior Under Reservoir Condition in Carbonate Acidizing

Ming Liu · Shicheng Zhang · Jianye Mou · Fujian Zhou

Received: 25 March 2012 / Accepted: 3 October 2012 / Published online: 11 October 2012

Abstract In carbonate reservoirs, acid is injected into the formation under breakdown pressure to react with the rock to remove the contaminations caused by drilling and production, which is called carbonate acidizing in reservoir development. In carbonate acidizing, acid flows selectively through large pores to create wormholes. Wormhole propagation under experimental condition has been studied by many experts. In this paper, a model which couples a two-scale continuum model simulating wormholing in the invaded zone and a reservoir flow model for the compressed zone was used to study the wormhole propagation behavior under reservoir condition. In this model, the porosity values which are uniformly distributed used in former literature follow the normal law. Based on the model, we first compared the results of the two porosity generation methods, and then studied the wormhole propagation behavior under reservoir condition, and finally simulated a two-layer formation to study the effects of distance and permeability ratio between the two layers. The results show that the normally distributed porosities simulate wormholing better. The effect of compressed zone on wormhole propagation increases with the decrease of compressibility factor and wormhole has a maximal value in length. The effect of distance between the two layers on wormhole lengths and acid distributions can be divided into three zones based on the wormhole length

This paper is dedicated to my father Kaizhen Liu and my mother Xi Wang.

M. Liu (✉) · S. Zhang · J. Mou
MOE Key Laboratory of Petroleum Engineering, China University of Petroleum, Beijing 102249, China
e-mail: liuming1104@gmail.com

S. Zhang
e-mail: zhangsc@cup.edu.cn

J. Mou
e-mail: moujianye@163.com

F. Zhou
Research Institute of Petroleum Exploration & Development, PetroChina, Beijing 100083, China
e-mail: zhoufujian@263.net

in the lower layer. A critical value of permeability ratio between the two layers exists, below and above which the wormhole length in the low permeability layer decreases sharply and almost keeps constant, respectively.

Keywords Carbonate acidizing · Wormhole · Reservoir condition · Compressed zone · Continuum model

List of Symbols

Variables

a_0	Initial average interfacial area per unit volume of the medium (m^{-1})
a_v	Interfacial area per unit volume of the medium (m^{-1})
A_v	Dimensionless interfacial area
C_f	Cup-mixing concentration of acid in the fluid phase ($mol\,L^{-1}$)
c_f	Dimensionless cup-mixing concentration of acid in the fluid phase
C_l	Formation fluid compressibility factor (MPa^{-1})
C_0	Initial concentration of acid ($mol\,L^{-1}$)
C_s	Concentration of acid at the solid–fluid interface ($mol\,L^{-1}$)
c_s	Dimensionless concentration of the acid at the fluid–solid interface
c_v	Coefficient of variation
Da	Damköhler number, ratio of reaction rate to mass transfer rate
D_m	Molecular diffusivity ($m^2\,s^{-1}$)
D_{eR}	Effective dispersion tensor in the radial direction ($m^2\,s^{-1}$)
$D_{e\theta}$	Effective dispersion tensor in the circumferential direction ($m^2\,s^{-1}$)
D_r	Dimensionless effective dispersion coefficient in the radial direction
D_θ	Dimensionless effective dispersion coefficient in the circumferential direction
$\hat{G}$	Standard Gaussian/normal distribution function
K	Permeability of the medium (μm^2)
K_0	Initial average permeability of the medium (μm^2)
k	Dimensionless permeability of the medium
K_{0h}	Initial average permeability in the high permeability layer (μm^2)
K_{0l}	Initial average permeability in the low permeability layer (μm^2)
k_c	Mass transfer coefficient ($m\,s^{-1}$)
k_s	Surface reaction rate constant ($m\,s^{-1}$)
m	Ratio of pore length to pore diameter
N_{ac}	Acid capacity number, the volume of solid dissolved per unit volume of the acid
p	Dimensionless formation pressure
P	Reservoir pressure (MPa)
P_e	Initial reservoir pressure (MPa)
Pe	Peclet number, ratio of diffusion time to convection time
P_r	Reservoir pressure in the compressed zone (MPa)
P_I	Pressure at the interface between the invaded zone and the compressed zone (MPa)
P_{bh}	Inlet pressure (MPa)
Re_p	Pore Reynolds number, ratio of inertial force to viscous force in the pore
r_w	Wellbore radius (m)
r_{invade}	Radius of the invaded zone (m)
r_e	Radius of the compressed zone (m)
r_p	Pore radius (m)
r_{po}	Initial average pore radius (m)

$R(C_s)$	Reaction kinetics ($m\,mol\,L^{-1}\,s^{-1}$)
Sc	Schmidt number, ratio of kinetic viscosity of the fluid to the molecular diffusivity
Sh	Sherwood Number, ratio of convective to diffusive mass transport
Sh_∞	Asymptotic Sherwood number for the pore
t'	Time (s)
t	Dimensionless time
u	Dimensionless velocity in the radial direction
$\|U\|$	Magnitude of the Darcy velocity ($m\,s^{-1}$)
u_0	injection velocity ($m\,s^{-1}$)
u_r	Darcy velocity in the radial direction ($m\,s^{-1}$)
u_θ	Darcy velocity in the circumferential direction ($m\,s^{-1}$)
v	Dimensionless velocity in the circumferential direction
v_s	Kinetic viscosity of the fluid ($m^2\,s^{-1}$)

Greek Symbols

α	Dissolving power of acid, defined as grams of solid dissolved per mole of acid reacted. (g/mol)
α_w	Dimensionless wellbore radius
$\alpha_{os}, \lambda_r, \lambda_\theta$	Numerical coefficients that depend on the structure of the medium
β	Exponent determined from experiment
ε	Porosity of the medium
ε_0	Initial average porosity of the medium
ζ_p	Dimensionless pore radius
η	Dimensionless initial pore diameter
μ	Viscosity of the acid (mPa s)
μ_f	Viscosity of the reservoir fluid (mPa s)
ξ	Dimensionless wormhole length in the radial direction
ρ_s	Density of the rock ($g\,cm^{-3}$)
ϕ^2	Pore scale Thiele modulus
Φ^2	Core scale Thiele modulus

1 Introduction

Carbonate reservoir is a very special kind of reservoir in petroleum industry. By definition, carbonate rocks contain more than 50 % carbonate minerals which usually mean calcite and dolomite. They present special physical characteristics, such as strong heterogeneity or double porosity, which are inherited from their process of formation. During oil and gas development, the near wellbore zone can be damaged by well drilling and completion, fines migration and other petroleum production operations, which hinders the flow of hydrocarbons into the well. Hydrochloric acid is usually used to react with the rock to create a high conductivity channel, namely wormhole, so that hydrocarbons can bypass the damaged zone. The process is called as carbonate acidizing.

Many researchers have studied the wormhole propagation behavior through experimental observations and analyses. Daccord et al. (1993a,b) studied the effect of injection rate on dissolution patterns through injecting water into plaster made cores. They found that there existed an optimal value to form wormholes. Breakthrough volume is defined as the ratio of injection volume to total pore volume. At very high injection rate, acid has insufficient

residence time to dissolve the rock so that the permeability of the cores cannot be increased significantly. At very low injection rate, acid dissolves rock completely to create large voids near the wellbore which may cause borehole collapse during production. Both of these conditions cost more acid than creating wormhole, that is, the breakthrough volume for creating wormhole is the least. Hoefner and Fogler (1988) also studied the effect of injection rate through injecting acid into limestone and dolomite cores and obtained similar results. Fredd and Fogler (1999) used different acid types to represent different reaction and mass transfer rates to study their effects on the condition of wormhole formation. It was found that the optimal injection velocity decreased as the acid-rock reaction changed from mass transfer control to reaction kinetics control. Other studies (Frick et al. 1994; Buijse 2000; Bazin 2001) were conducted to investigate the influences of acid concentration, medium heterogeneity, and core size.

Other researchers (Hung et al. 1989; Liu et al. 1997; Huang et al. 1997, 1999; Gdanski 1999; Buijse 2000; Golfier et al. 2002) have used mathematical modeling to simulate wormhole propagation behavior. Earlier literature used capillary tube model and network model to study the effects of fluid leakage, reaction kinetics and wormhole density on wormhole propagation. The capillary tube model assumes wormhole as a capillary tube. Due to the simple structure, the model neglects transport mechanism and pore-scale reaction. The network model represents the porous medium as a network of tubes interconnected to each other at the nodes. The wormhole growth in the transverse direction is represented by enlargement of the tube radius. Though dissolution patterns and qualitative features of dissolution are captured by this model, it is found that the simulated acid injection volume is much higher than that observed in experiments. Kang et al. (2002) developed a lattice Boltzmann model to simulate the dynamic process of convection, diffusion and reaction in porous media. Applying this model to simulate carbonate acidizing, significant experimental observations are verified and confirmed. In recent works, a two-scale continuum model was developed to improve the simulation results. This model is based on both Darcy scale and pore scale. The Darcy scale model describes reaction and dissolution and the pore scale model describes the pore structure change due to dissolution. Coupling the two models and adding initial and boundary conditions, we can numerically solve them. Panga (2003) and Panga et al. (2005) studied the effect of medium heterogeneity on wormhole propagation in linear flow. Kalia and Balakotaiah (2007); Kalia and Balakotaian (2009) extended the model to polar coordinate to simulate radial flow and further studied the effects of heterogeneity, fractal nature and pressure response with the radial model. Izgec et al. (2008, 2009) studied acid flow in vuggy carbonates with different vug distribution patterns, but the reaction mechanism is not considered.

Although the results of this two-scale continuum model can accord well with the experimental observations, there are three important drawbacks when the reservoir condition is taken into account. First, the method to generate porosities is not appropriate for carbonates which usually have strong heterogeneity. The wormholes obtained from the simulations which are usually straight are slightly different from those obtained from the core experiments whose traces are usually irregularly changed due to the strong heterogeneity (Tardy et al. 2007). Second, injected acid displaces reservoir fluid in the pore to dissolve the rock, which makes the reservoir fluid compressed under reservoir condition. With the increase of injection volume, the effect of compressed reservoir fluid on wormhole propagation cannot be neglected. Third, it takes different time for acid to arrive at different layer when multilayer formation is stimulated by acidization. The wormholes are firstly created in the layer which receives acid early. With the injection of acid, wormhole propagates faster and more acid flows into this layer, which would have an important impact on wormhole propagation

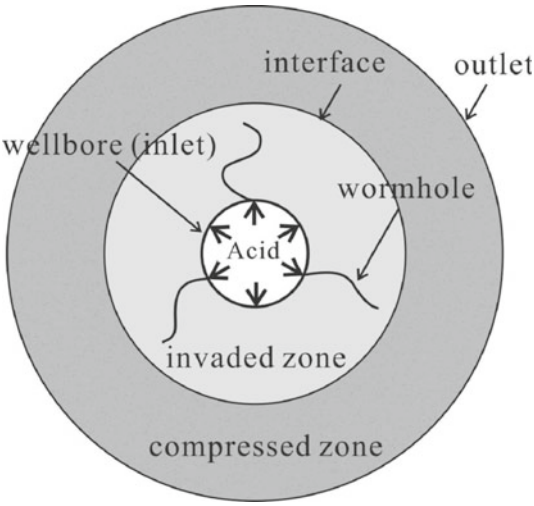

Fig. 1 Schematic diagram of wormhole propagation in polar coordinate

in other layers. Cohen et al. (2008) explained this phenomenon from two mechanisms, the diffusion effect and the shadowing effect.

In this paper, we couple the two-scale continuum model with a reservoir flow model to simulate the wormhole propagation behavior under reservoir condition. First, the normal distribution method is introduced to generate porosities and compared with the uniform distribution method. Second, we separately set constant rate and pressure boundaries at the inlet to simulate wormhole propagation behavior and analyze the results. Third, we simulate a two-layer formation acidization to study the effects of distance and permeability ratio between the two layers on wormhole propagation.

2 Mathematical Model

As shown in Fig. 1, acid is injected down the wellbore into the formation. With the acid-rock reaction, wormholes are formed in the invaded zone and reservoir fluids are squeezed into the compressed zone. Due to lack of sufficient computation power, we simulate 2D radial flow in these two zones.

2.1 Invaded Zone

In the invaded zone, we use a two-scale continuum model to simulate acid flow, acid-rock reaction and porosity change. The details have been discussed by Kalia and Balakotaiah (2007). A difference in our model is the method to generate the porosity field. Since geostatistical researches have shown the porosity distribution follows the normal law (Chierici 1994; Greenkorn 1983; Hollis et al. 2010; Schoenfelder et al. 2008), we use a normal distribution function to generate the porosity field.

2.1.1 Darcy Scale Model

The Darcy scale model which considers convection, diffusion, and reactive dissolution is given by:

$$(u_r, v_\theta) = -\frac{K}{\mu}\left(\frac{\partial P}{\partial r}, \frac{1}{r}\frac{\partial P}{\partial \theta}\right) \tag{1}$$

$$\frac{\partial \varepsilon}{\partial t'} + \frac{1}{r}\frac{\partial}{\partial r}(r u_r) + \frac{1}{r}\frac{\partial u_\theta}{\partial \theta} = 0 \tag{2}$$

$$\begin{aligned}&\frac{\partial(\varepsilon C_f)}{\partial t'} + \frac{1}{r}\frac{\partial}{\partial r}(r u_r C_f) + \frac{1}{r}\frac{\partial}{\partial \theta}(u_\theta C_f)\\ &= \frac{1}{r}\frac{\partial}{\partial r}\left(r\varepsilon D_{eR}\frac{\partial C_f}{\partial r}\right) + \frac{1}{r}\frac{\partial}{\partial \theta}\left(\frac{\varepsilon D_{e\theta}}{r}\frac{\partial C_f}{\partial \theta}\right) - k_c a_v (C_f - C_s)\end{aligned} \tag{3}$$

$$k_c(C_f - C_s) = R(C_s) = k_s C_s \tag{4}$$

$$\frac{\partial \varepsilon}{\partial t'} = \frac{R(C_s) a_v \alpha}{\rho_s} \tag{5}$$

Equations (1)–(3) are Darcy percolation equation, continuity equation and convection-diffusion equation, respectively. The last term at R.H.S. of Eq. (3) represents mass transfer. Equation (4) balances the amount of reactant transferred to the solid surface to the amount reacted. Eq. (5) describes the evolution of porosity due to reaction.

Since the model depends on chemical reaction, we use dimensionless form to identify several important chemical parameters. The dimensionless parameters used are defined in Eq. (6). Equations (1)–(5) are non-dimensionalized as Eqs. (7)–(10).

$$\begin{aligned}&\xi = \frac{r}{r_{invade}}, \alpha_w = \frac{r_w}{r_{invade}}, u = \frac{u_r}{u_0}, v = \frac{u_\theta}{u_0}, t = \frac{t'}{r_{invade}/u_0}, \zeta_p = \frac{r_p}{r_{po}}, A_v = \frac{a_v}{a_0},\\ &k = \frac{K}{K_0}, c_f = \frac{C_f}{C_0}, c_s = \frac{C_s}{C_0}, p = \frac{P - P_e}{\frac{\mu u_0 r_{invade}}{K_0}}, \eta = \frac{2r_{po}}{r_{invade}}, \phi^2 = \frac{2k_s r_{po}}{D_m},\end{aligned} \tag{6}$$

$$Da = \frac{k_s a_0 r_{invade}}{u_0}, N_{ac} = \frac{\alpha C_0}{\rho_s}, Pe = \frac{u_0 r_{invade}}{D_m}, \Phi^2 = Da \cdot Pe = \frac{k_s a_0 r_{invade}^2}{D_m}$$

$$(u, v) = -\left(k\frac{\partial p}{\partial \xi}, \frac{k}{\sigma}\frac{\partial p}{\partial \theta}\right) \tag{7}$$

$$\frac{\partial \varepsilon}{\partial t} - \frac{1}{\xi}\frac{\partial}{\partial \xi}\left(\xi k\frac{\partial p}{\partial \xi}\right) - \frac{1}{\xi}\frac{\partial}{\partial \theta}\left(\frac{k}{\xi}\frac{\partial p}{\partial \theta}\right) = 0 \tag{8}$$

$$\begin{aligned}&\frac{\partial(\varepsilon c_f)}{\partial t} + \frac{1}{\xi}\frac{\partial}{\partial \xi}(\xi u c_f) + \frac{1}{\xi}\frac{\partial}{\partial \theta}(v c_f) = \frac{1}{\xi}\frac{\partial}{\partial \xi}\left(\xi D_r\frac{\partial c_f}{\partial \xi}\right)\\ &+\frac{1}{\xi}\frac{\partial}{\partial \theta}\left(\frac{D_\theta}{\xi}\frac{\partial c_f}{\partial \theta}\right) - \frac{Da A_v c_f}{1 + \frac{\phi^2 \zeta_p}{Sh}}\end{aligned} \tag{9}$$

$$\frac{\partial \varepsilon}{\partial t} = \frac{Da N_{ac} A_v c_f}{1 + \frac{\phi^2 \zeta_p}{Sh}} \tag{10}$$

In dimensionless form, the boundary and initial conditions are:

$$p = \frac{P_{bh} - P_e}{\frac{\mu u_0 r_{invade}}{K_0}}, c_f = 1 \quad \text{at } \xi = \alpha_w \tag{11}$$

$$-k\frac{\partial p}{\partial \xi} = 1, c_f = 1 \quad \text{at } \xi = \alpha_w \tag{12}$$

$$p = \frac{P_l - P_e}{\frac{\mu u_0 r_{invade}}{K_0}}, \frac{\partial c_f}{\partial \xi} = 0 \quad \text{at } \xi = 1 \tag{13}$$

$$c_f = 0 \quad \text{at } t = 0 \tag{14}$$

$$\varepsilon = \begin{cases} 0.99, & \varepsilon \geq 0.99 \\ \varepsilon_0 + \varepsilon_0 c_v \hat{G}, 0.005 < \varepsilon < 0.99 & \text{at } t = 0 \\ 0.005, & \varepsilon \leq 0.005 \end{cases} \tag{15}$$

$$p(\xi, \theta) = p(\xi, \theta + 2\pi), c_f(\xi, \theta) = c_f(\xi, \theta + 2\pi) \quad \text{at } \theta = 0 \tag{16}$$

Equations (11) and (12) represent constant pressure and rate conditions, respectively. During simulation, either Eq. (11) or (12) is used for solving the set of equations. From Eq. (15), porosities are generated with two threshold values. Considering the normal law, porosity values will be smaller than zero and bigger than one when the initial porosity value and the coefficient of variation are relatively large. To validate the simulation, we set 0.005 and 0.99 as the minimal and maximal threshold values. Any values smaller and bigger than the minimal and maximal threshold values will be set as 0.005 and 0.99, respectively. Although this would leads to an asymmetric probability distribution, the effect can be negligible because the number of values which are smaller than 0.005 and bigger than 0.99 are very few. $\hat{G}$, which is the standard normal distribution function, generates a certain number of random numbers.

2.1.2 Pore Scale Model

The pore scale model is used to describe the pore structure–property relationship. Since the dissolution on Darcy scale changes the pore structure continuously, it is impractical to find a precise relationship between the change of pore properties and that of pore structure. A series of qualified semi-empirical equations are needed. In Panga's work (Panga et al. 2005), they are shown as:

$$k = \frac{\varepsilon}{\varepsilon_0}\left(\frac{\varepsilon}{\varepsilon_0}\left(\frac{1-\varepsilon_0}{1-\varepsilon}\right)\right)^{2\beta} \tag{17}$$

$$\zeta_p = \sqrt{k\frac{\varepsilon_0}{\varepsilon}} \tag{18}$$

$$A_v = \frac{\varepsilon}{\zeta_p \varepsilon_0} \tag{19}$$

The mass transfer coefficient, k_c, depends on the porosity, permeability, reaction rate and fluid velocity. Balakotaiah and West (2002) investigated the effects of these parameters on mass transfer coefficient and obtained the following equation:

$$Sh = \frac{2k_c r_p}{D_m} = Sh_\infty + \frac{0.7}{m^{1/2}} Re_p^{1/2} Sc^{1/3}, \tag{20}$$

where Sh $(= 2k_c r_p / D_m)$ is the Sherwood number, defined as the ratio of convective to diffusive mass transport; $\mathrm{Re}_p (= 2u_0 r_{po}/\nu_s)$ is the pore Reynolds number, defined as the ratio of inertial force to viscous force in the pore; $(Sc = \nu_s / D_m)$ is the Schmidt number, defined as the ratio of kinetic viscosity of the fluid to the molecular diffusivity.

The effective dispersion coefficients in r and θ direction are calculated as:

$$D_r = \frac{\alpha_{os} \varepsilon Da}{\Phi^2} + \lambda_r |U| \zeta_p \eta \quad D_\theta = \frac{\alpha_{os} \varepsilon Da}{\Phi^2} + \lambda_\theta |U| \zeta_p \eta. \tag{21}$$

Table 1 Model parameters and corresponding values

K_0	ε_0	μ	μ_f	r_{invade}	r_w	β	k_s	D_m	r_{po}	a_0	α	C_0	ρ_s	ρ_l
0.01	0.15	0.01	0.005	0.4	0.1	1	2×10^{-3}	3×10^{-9}	1	50	50	4.4	2,500	1,000
μm^2	–	Pa s	Pa s	m	m	–	m/s	m^2/s	10^{-6}m	cm^{-1}	g/mol	mol/L	kg/m^3	kg/m^3

2.2 Compressed Zone

As the acid is injected into the formation, the wormholes are created and the formation fluid is compressed. The process of compression can be expressed by the following differential equation and boundary conditions with dimensional forms:

$$\frac{1}{r}\frac{\partial}{\partial r}\left(r\frac{\partial P_r}{\partial r}\right)=\frac{\varepsilon\mu_f C_l}{K}\frac{\partial P_r}{\partial t'} \tag{22}$$

$$P_r = P_I \quad \text{at } r = r_{\text{invade}} \tag{23}$$

$$P_r = P_e \quad \text{at } r = r_e \tag{24}$$

$$P_r = P_e \quad \text{at } t' = 0 \tag{25}$$

2.3 Numerical Solution

For feasibility, the model equations are discretized with finite volume discretization method to satisfy the conservation of mass, momentum and species and solved sequentially. First, the continuity equation is solved to get the velocity and pressure fields, then the convection-diffusion equation is solved to get the acid concentration distribution, then pore properties are updated through solving the pore scale model, then the reservoir pressure model is solved to get the pressure distribution in the compressed zone, and finally the pressure at the interface between the invaded zone and the compressed zone is updated. The model has been validated by Panga et al. (2005) and Kalia and Balakotaiah (2007). The parameters used for solution are listed in Table 1, all values are fixed unless otherwise stated. The definition of breakthrough plays an important role in influencing the value of breakthrough volume. In the former literature, breakthrough is defined as decrease in the pressure drop by a factor of 100 from the initial pressure drop. However, this is only correct when created channels are wide enough such as dominant wormhole and face dissolution, Figs. 2b and 3c. For uniform dissolution and ramified wormholes, Fig. 3a, b, acid breaks through the medium before the inlet pressure drop decreases to 1 % of the initial pressure drop due to the wide acid front and thin channel. Through a series of simulations, we find 10 % of acid concentration is a proper value as the criterion, below which the breakthrough volumes hardly change. Therefore, breakthrough is defined as increase in the acid concentration of the interface by 10 % from the initial acid concentration in this work.

3 Results and Discussion

3.1 Normally Distributed Porosities

In Panga's model, the porosity values are generated by adding a group of random numbers uniformly distributed in the interval $[-\Delta\varepsilon_0, \Delta\varepsilon_0]$ to the mean value of porosity ε_0. However,

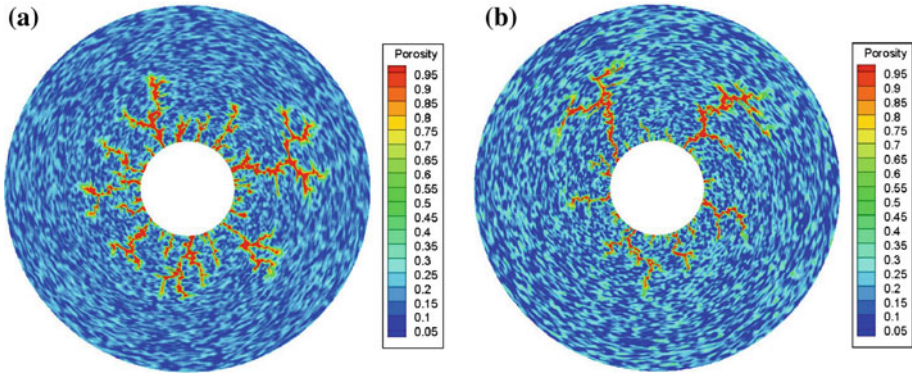

Fig. 2 Dissolution patterns visible in porosity contour plots at the optimal injection velocity for **a** uniformly distributed porosities and **b** normally distributed porosities

it is not consistent with the real distribution in cores whose porosities follow the normal law. In this section, we use a normal distribution method to generate the initial porosity field, Eq. (15). Then, the wormhole structure and breakthrough volume are compared to prove our method is more reasonable. The porosity values for uniform distribution method are generated by adding a group of random fluctuations uniformly distributed in the interval $[-0.145, 0.145]$ to 0.15 to express strong heterogeneity. The normally distributed porosity values are generated by Eq. (15) at $c_v = 1.0$. Therefore, the minimal porosity values for the two methods are equal and the maximal value for normal distribution method is bigger.

In Fig. 2, dissolution patterns for the two different porosity distribution methods are shown at the optimal injection velocity. Acid selectively flows into the big pores to create wormholes for both of the two cases. However, it is important that the wormhole structures and densities are very different from each other. For uniformly distributed porosities, the wormholes are evenly developed so as to have a great density. For normally distributed porosities, two dominant wormholes are developed. From the experimental observations, wormholes are commonly developed like the case (b) due to the strong heterogeneity in carbonates (Tardy et al. 2007) and the optimal breakthrough volume is about one or less (Fredd and Fogler 1999; Bazin 2001). From Fig. 3, the optimal breakthrough volumes for normally distributed porosities are 1.48 at $\varepsilon_0 = 1.5$ and 0.52 at $\varepsilon_0 = 3.0$, respectively. Apparently, the results are much closer to the experimental ones than uniformly distributed porosities. Fig. 4 shows the comparison of the experimental data with the two porosity distribution methods. In the figure, the experimental data are from Fredd and Fogler (1999) and the breakthrough curves are obtained from simulations. It is shown that the breakthrough curve and the optimal breakthrough volume for the normally distributed porosities are closer to the experimental data. Since the model used is 2D, the heterogeneity is smaller than that of real 3D cores so that the wormhole propagation velocity is slower, which leads to a bigger optimal breakthrough volume. The study on 3D model will be pursued in the future work.

In addition, we can see from the arrow direction in Fig. 3 that the optimal Damköhler number increases with the increase of heterogeneity. For uniformly distributed porosities, the optimal Damköhler number is 500. For normally distributed porosities, the optimal Damköhler numbers are 1,000 at $\varepsilon_0 = 0.15$ and 2,000 at $\varepsilon_0 = 0.3$, respectively. Since the Damköhler number is inversely proportional to the injection velocity, the increase of heterogeneity decreases the optimal injection velocity. With the decrease of injection velocity, dissolution

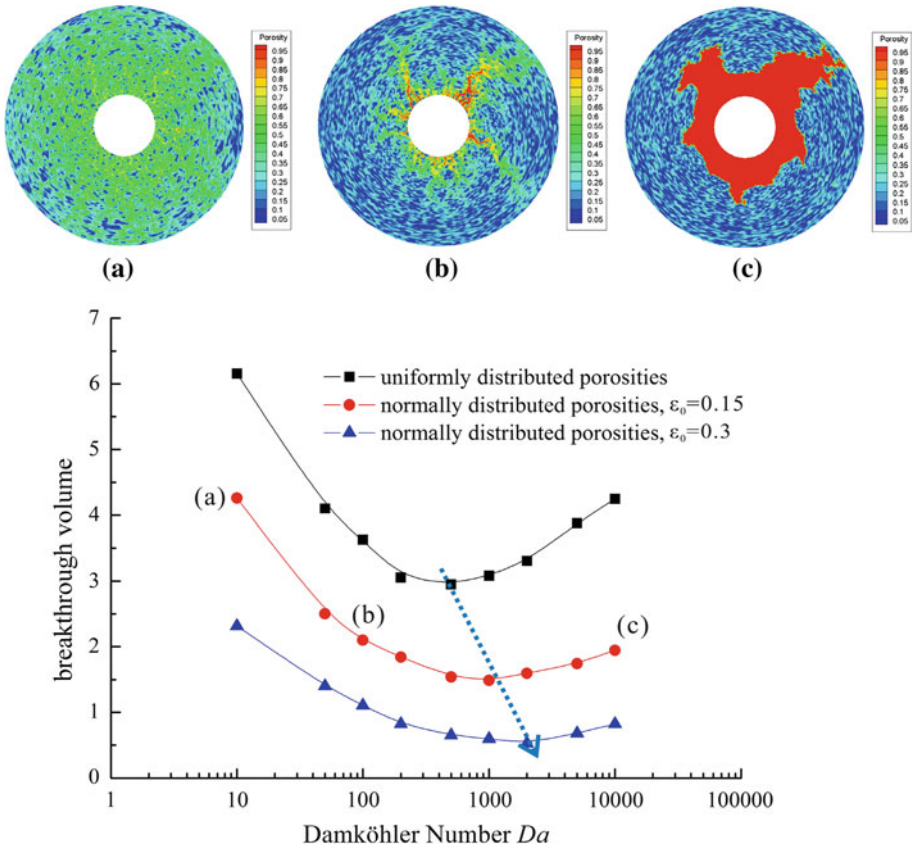

Fig. 3 Breakthrough curves for the two different porosity generation methods: **a** uniform dissolution, **b** ramified wormholes, and **c** face dissolution

patterns change from uniform dissolution (Fig. 3a), ramified wormhole (Fig. 3b), dominant wormhole (Fig. 2b) to face dissolution (Fig. 3c).

The created different dissolution patterns depend on both convection effect and diffusion effect. At high injection rate, the convection effect dominates the flow process and the diffusion effect is relatively weak. The acid tends to flow in the radial direction other than the circumferential direction, which leads to insufficient reaction time. The uniform dissolution is formed. At low injection rate, the diffusion effect dominates the flow process and the convection effect is relatively weak. The acid has enough time to react with the rock before flowing forward so that face dissolution is created. At intermediate injection rate, the diffusion effect and convection effect are of order unity. Acid flows forward with a relatively big velocity while dissolving the rock, which creates the wormholes.

3.2 Effect of Boundary Conditions

In carbonate acidizing, acid is usually injected down the wellbore at constant rate. Since wormhole formation depends on the injection velocity, the wormhole propagation velocities are the same with or without considering the compressed zone. However, the interface pressure between the invaded zone and the compressed zone changes with the fluid

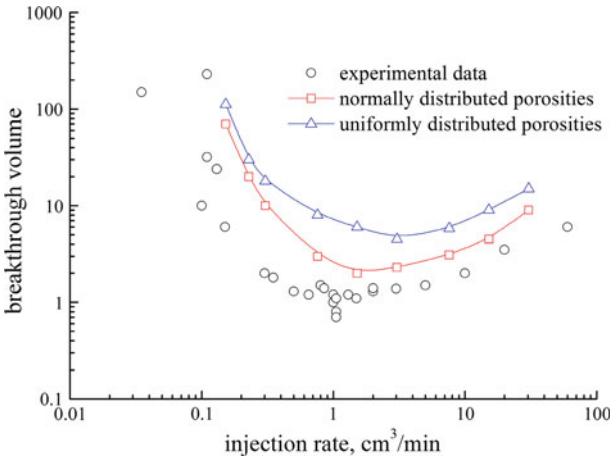

Fig. 4 Comparison of experimental data with two different porosity distribution methods at $C_0 = 0.5\,\text{mol/L}$ and $\varepsilon_0 = 0.2$

compressibility factor. So, the constant rate boundary is used to study the effect of the compressibility factor on the interface pressure. In addition, the injection rate would change with the formation of wormholes if the constant pressure is imposed at the inlet. Therefore, to study the effect of changing injection rate on wormhole propagation behavior, the constant pressure boundary is also investigated.

3.2.1 Constant Rate Boundary

Under experimental condition, acid is injected at constant rate into the cores with the outlet pressure equaling to the atmospheric pressure. With the formation of wormholes, the pressure difference between the inlet and the outlet decreases. However, under reservoir condition, the pressure difference which denotes the one between the inlet and the interface depends on the injection rate and reservoir compressibility factor. Since wormhole is created at certain injection rate, the reservoir compressibility factor is the most important factor to influence the wormhole propagation behavior. Fig. 5 shows the inlet pressures and interface pressures changing with the injection time. In this figure, $C_l = 0.002\,\text{MPa}^{-1}$ and $C_l = 0.02\,\text{MPa}^{-1}$ represent the reservoir conditions with different compressibility factors and $C_l = \infty$ represents the experimental condition. From the figure, the inlet pressures decline more slowly and the interface pressures increase more quickly with the decrease of formation fluid compressibility factor. At $C_l = \infty$, since the compressed zone is not considered, the interface pressure equals to zero. As the reservoir fluid is forced to flow back into the compressed zone, small compressibility factor produces big pressure increase at the interface. In order to inject acid at the fixed rate, the inlet pressure needs to decline more slowly compared to the experimental condition. One important result can be anticipated that there exists a maximal wormhole length for a certain compressibility factor when the pressure difference decreases to a certain value.

3.2.2 Constant Pressure Boundary

Constant pressure boundary means a constant injection pressure is imposed at the inlet and the injection rate is changed according to the pressure difference between the inlet and the

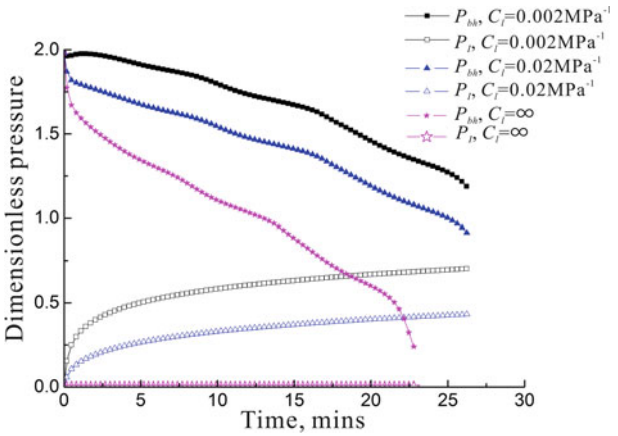

Fig. 5 Inlet and interface pressures change with the injection time at the optimal injection velocity

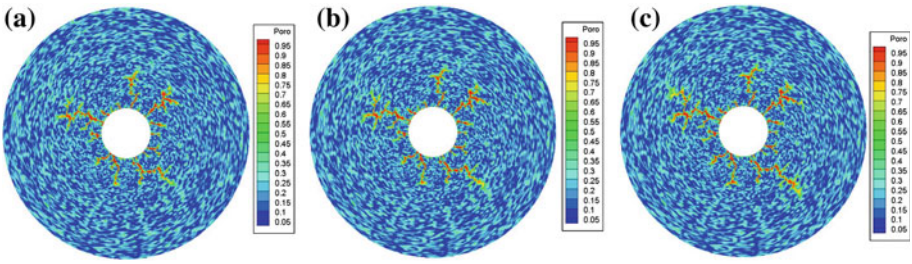

Fig. 6 Dissolution patterns in porosity for different compressibility factors: **a** $C_l = 0.002\,\mathrm{MPa}^{-1}$, **b** $C_l = 0.02\,\mathrm{MPa}^{-1}$, and **c** $C_l = \infty$

interface. Figures 6 and 7 show the porosity distribution patterns and pressure distribution patterns for different compressibility factors after injecting acid for 30 min. Since the compressed zone is much larger than the invaded zone, for clarity, only the invaded zone is shown in the figures. From Fig. 6, the wormhole length increases with the compressibility factor. From Fig. 7, we can see that the interface pressure increases with the decrease of compressibility factor. Obviously, the increase of interface pressure decreases the pressure difference, which decreases the injection rate. As a result, the wormhole propagates slower under reservoir condition than that under experimental condition. Again, there exists a maximal wormhole length under constant pressure boundary condition due to the continuous decrease of the pressure difference.

3.3 Two-Layer Formation Acidizing

In general, hydrocarbons are usually distributed in the way as shown in Fig. 8 that the hydrocarbon-bearing layers are isolated by dry layers. In this section, a two-layer formation which means two hydrocarbon-bearing layers with a dry layer between them is simulated to investigate the effects of distance and permeability ratio on wormhole lengths and acid distributions under constant rate condition. We assume that the wellbore is filled with reservoir fluid in advance. Since wormhole is usually viewed as the infinite conductivity channel in which

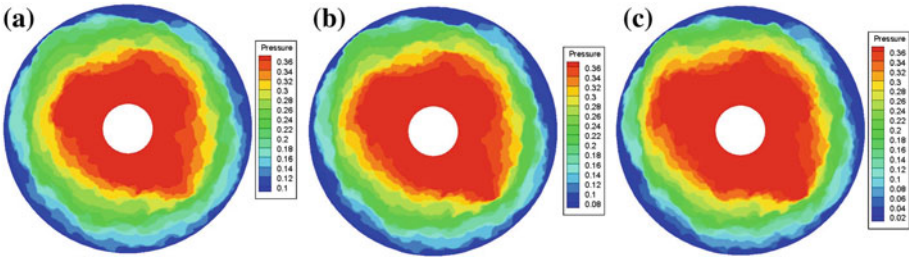

Fig. 7 Dimensionless pressure distributions for different compressibility factors: **a** $C_l = 0.002\,\mathrm{MPa}^{-1}$. **b** $C_l = 0.02\,\mathrm{MPa}^{-1}$, and **c** $C_l = \infty$

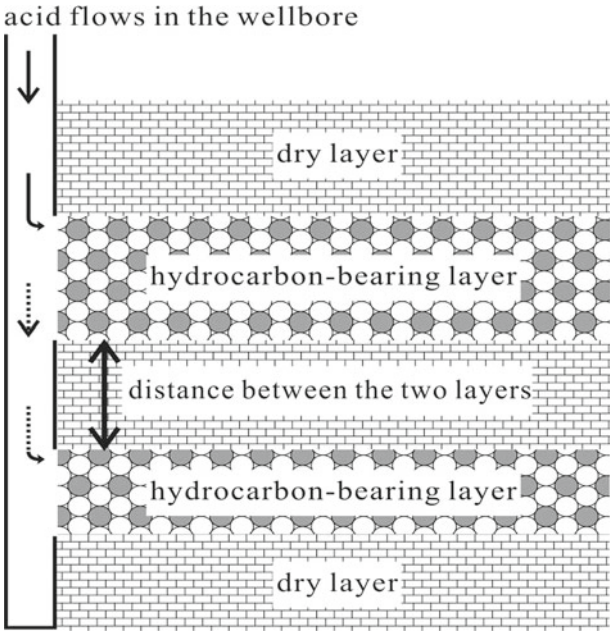

Fig. 8 Underground hydrocarbon-bearing layers and acid flow schematic diagram

the pressure drop is negligible, we define channel whose porosities are bigger than 0.7 as wormhole. Wormhole length is the length of the longest wormhole in the radial direction.

3.3.1 Effect of Distance Between the Two Layers

Depending on a distance between the two layers, the upper layer receives acid before the acid arrives at the lower layer. As we can imagine, the distance between the two layers has an important effect on the wormhole lengths in these layers. To remove the effect of permeability difference, we assume the same permeability fields (or porosity fields) in both layers. Figures 9 and 10 show the wormhole lengths and acid distributions in both layers with different distances under reservoir condition and experimental condition, respectively. Before the analyses, two concepts should be clarified, the wormholing effect and the compressed zone effect. The wormholing effect means the effect of wormhole propagation. Stronger

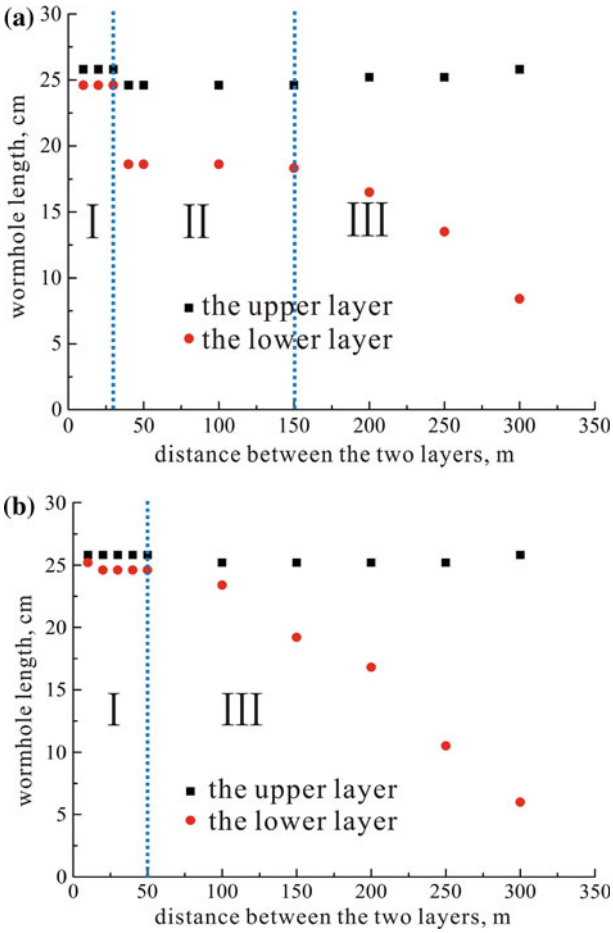

Fig. 9 Wormhole lengths in the two layers with different distances under different conditions: **a** reservoir condition and **b** experimental condition

wormholing effect means the wormhole propagates faster. The compressed zone effect depends on the compressibility factor of formation fluid. Small compressibility factor denotes strong compressed zone effect. From Fig. 9a, three zones can be identified based on different wormhole lengths in the lower layer. Under reservoir condition, the wormhole length in the lower layer is not only dependent on the wormholing effect but also dependent on the compressed zone effect. Since the upper layer receives acid earlier than the lower layer, wormholes are created in the upper layer at first. So, the acid prefers to flow into this layer and the wormholing effect becomes stronger. In zone I, the wormhole lengths in both layers are close. It is because the distance is so small that the wormholing effects in the two layers are of order unity. From Fig. 10a, the acid rates in both layers are almost the same when the distance is 10m. In zone II, wormhole length in the lower layer is smaller but remains constant with the increase of distance. From Fig. 10a, the acid rate in the lower layer decreases with the injection of acid when the distance is 50 m, which forms a shorter wormhole. What interesting is that the wormhole length difference remains constant in a certain distance range, from 30 to 150 m in this case. It indicates that a balanced acid distribution for both layers exists.

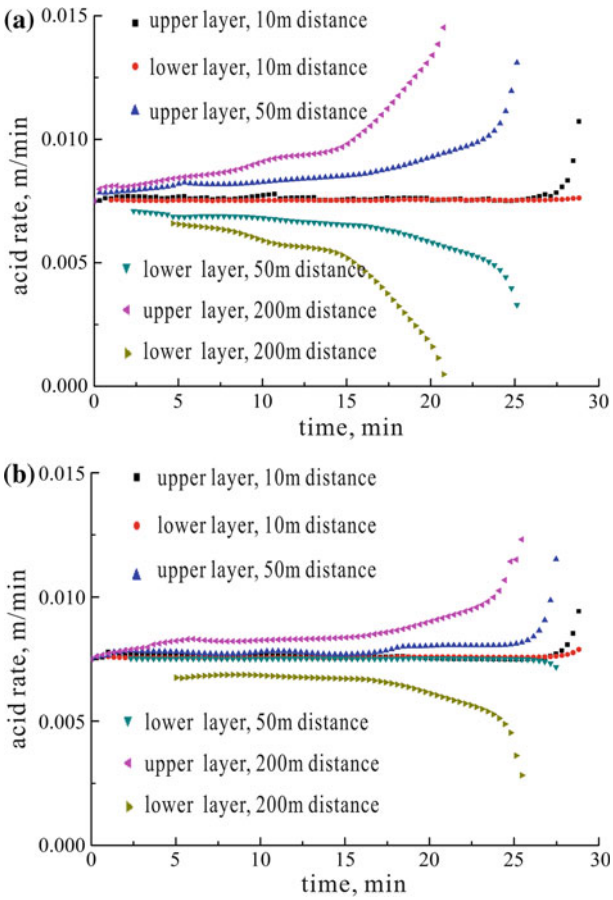

Fig. 10 Acid distributions in the two layers with different distances under different conditions: **a** reservoir condition at $C_1 = 0.002\,\mathrm{MPa}^{-1}$ and **b** experimental condition

In this range, the pressure increase at the inlet due to the increase of acid rate equals to the pressure decline due to the increase of wormhole length. In zone III, wormhole lengths in the lower layer decreases with the increase of distance. From Fig. 10a, the acid rate in the lower layer decreases sharply with the injection of acid when the distance is 200 m. This means that a relatively long wormhole is formed in the upper layer before the acid arrives at the lower layer. The pressure decline at the inlet due to the increase of wormhole length plays a more dominant role than the pressure increase due to the increase of acid rate in influencing the acid distribution between the two layers. Under experimental condition, however, only zone I and zone III exist. From Fig. 9b, the wormhole length in the lower layer and the distance follow a linear relationship in zone III. It is because that the wormhole length in the lower layer is only dependent on the wormholing effect. From Fig. 10b, the acid rate in the lower layer decreases slightly with the distance increasing from 10 to 50 m, and decreases sharply with the distance increasing from 50 to 200 m.

From the above analyses, we can see that the wormhole length under reservoir condition has a very different relationship with the distance compared to the experimental condition.

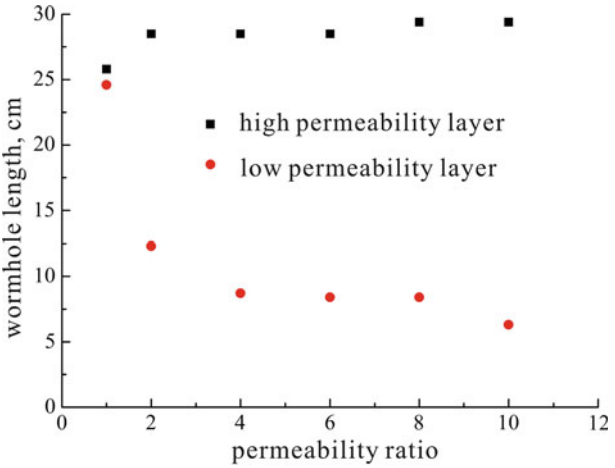

Fig. 11 Effect of permeability ratios on wormhole lengths

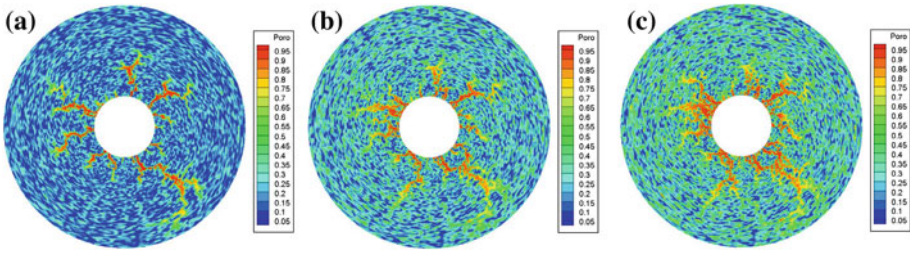

Fig. 12 Dissolution patterns in high permeability layer at **a** $K_{0h}/K_{0l} = 1$, **b** K_{0h}/K_{0l}=4, and **c** K_{0h}/K_{0l}=8

The most important difference is that the maximal distance required to keep the wormhole lengths in both layers close is smaller in the presence of the compressed zone. As a result, knowing its value is very important for petroleum engineers to choose their acidizing methods under different conditions. Taking thin inter-bedded reservoir for example, due to the small distance between the layers, wormhole lengths are close so that all layers can be well treated. However, we should isolate one layer at a time and treat it if the distance between the layers is too big.

3.3.2 Effect of Permeability Ratio

Due to different depositional mode, different layer usually has different average permeability. To study the effect of permeability difference on wormhole lengths, we assume acid arrives at each layer at the same time to remove the influence of the distance. Permeabilities and porosities are calculated with Eq. (17) on the basis of the given initial average permeability and porosity shown in Table 1. Permeability ratio, K_{0h}/K_{0l}, is defined as the ratio of a high permeability to a low permeability which is set as $10 \times 10^{-3}\ \mu m^2$. We simulate different permeability ratio ranging from one to ten to consider the strong heterogeneity in carbonate reservoirs. Figure 11 shows that the wormhole lengths in both layers change with the permeability ratios. From Fig. 11, wormhole lengths in the low permeability layers decrease sharply with the permeability ratio increasing from one to two and slowly afterwards. With the increase of permeability ratio, the high permeability layer receives more acid and the

interface pressure increases quickly. Since the optimal injection velocity decreases with the increase of heterogeneity (or porosity), Fig. 3, the ramified wormholes are created in the high permeability layer with the increase of acid rate, which leads to an imperfect stimulation for both layers, Fig. 12. Therefore, there is a balance point between the wormholing effect and the compressed zone effect when permeability ratio increases to a certain value.

4 Conclusions

In this paper, a model coupling a two-scale continuum model and a reservoir flow model was used to study the effects of two different boundary conditions and distance and permeability ratio in a two-layer formation on wormhole propagation behavior. Through a series of simulations, the following conclusions are achieved.

1. To compare with the uniform distribution method used in the former literature, the wormhole structure and the optimal breakthrough volume obtained from the normal distribution method are closer to the experimental observations.
2. With the increase of heterogeneity, the optimal injection velocity which creates wormholes decreases.
3. Under constant rate condition, the inlet pressure declines more slowly and the interface pressure increases more quickly with the decrease of compressibility factor. Under constant pressure condition, the wormhole propagation velocity decreases with the decrease of compressibility factor. For both cases, a maximal wormhole length exists because of the compressed zone effect.
4. In a two-layer formation, the effect of distance between layers can be divided into three zones. In zone I, the wormhole lengths in both layers are very close. In zone II, a balance between the wormholing effect and compressed zone effect exists so that the wormhole length in the lower layer keeps constant with the increase of distance. In zone III, the distance is so big that the lower layer can not be well treated before breakthrough in the upper layer. As the permeability ratio increases from one to two, wormhole length in the low permeability layer decreases sharply. After that, wormhole length in the low permeability layer almost keeps constant.

Acknowledgments The authors gratefully acknowledge the sponsor of the Project supported by National Natural Science Foundation of China, No. 51274213.

References

Balakotaiah, V., West, D.H.: Shape normalization and analysis of the mass transfer controlled regime in catalytic monoliths. Chem. Eng. Sci. **57**(8), 1269–1286 (2002)

Bazin, B.: From matrix acidizing to acid fracturing: a laboratory evaluation of acid/rock interactions. SPE Prod. Facil. **16**(1), 22–29 (2001)

Buijse, M.A.: Understanding wormholing mechanisms can improve acid treatments in carbonate formations. SPE Prod. Facil. **15**(3), 168–175 (2000)

Cohen, C.E., Ding, D., Quintard, M., Bazin, B.: From pore scale to wellbore scale: impact of geometry on wormhole growth in carbonate acidization. Chem. Eng. Sci. **63**(12), 3088–3099 (2008)

Daccord, G., Lenormand, R., Lietard, O.: Chemical dissolution of a porous medium by a reactive fluid-1. model for the "wormholing" phenomenon. Chem. Eng. Sci. **48**(1), 169–178 (1993a)

Daccord, G., Lenormand, R., Lietard, O.: Chemical dissolution of a porous medium by a reactive fluid-2. Convection vs reaction, behavior diagram. Chem. Eng. Sci. **48**(1), 179–186 (1993b)

Chierici, G.L.: Principles of Petroleum Reservoir Engineering, Vol. 1. Springer, Berlin (1994)

Fredd, C.N., Fogler, H.S.: Optimum conditions for wormhole formation in carbonate porous media: influence of transport and reaction. SPE J. **4**(3), 196–205 (1999)

Frick, T.P., Mostofizadeh, B., Economides, M.J.: Analysis of radial core experiments for hydrochloric acid interaction with limestones. SPE27402. Presented at SPE International Symposium on Formation Damage Control, Lafayette, Louisiana, 7–10 February 1994

Gdanski, R.: A fundamentally new model of acid wormholing in carbonate. In: SPE European Formation Damage Conference, The Netherlands, 31 May–01 June 1999

Golfier, F., Zarcone, C., Bazin, B., Lenormand, R., Lasseux, D., Quintard, M.: On the ability of a Darcy-scale model to capture wormhole formation during the dissolution of a porous medium. J. Fliud Mech. **457**, 213–254 (2002)

Greenkorn, R.A.: Flow Phenomena in Porous Media: Fundamentals and Applications in Petroleum, Water, and Food Production. Marcel Dekker, New York (1983)

Hoefner, M.L., Fogler, H.S.: Pore evolution and channel formation during flow and reaction in porous media. AIChE J. **34**(1), 45–54 (1988)

Hollis, C., Vahrenkamp, V., Tull, S., Mookerjee, A., Taberner, C., Huang, Y.: Pore system characterisation in heterogeneous carbonates: an alternative approach to widely-used rock-typing methodologies. Mar. Pet. Geol. **27**(4), 772–793 (2010)

Huang, T., Hill, A.D., Schechter, R.: Reaction rate and fluid loss: the keys to wormhole initiation and propagation in carbonate acidizing. SPE37312. Presented at SPE International Symposium on Oilfield Chemistry, Houston, Texas, 18–21 February 1997

Huang, T., Zhu, D., Hill, A.D.: Prediction of Wormhole population density in carbonate matrix acidizing. SPE54723. Presented at SPE European Formation Damage Conference, Hague, 31 May–01 June 1999

Hung, K.M., Hill, A.D., Sepehrnoori, K.: Mechanistic model of wormhole growth in carbonate matrix acidizing and acid fracturing. JPT **41**(1), 59–66 (1989)

Izgec, O., Keys, R., Zhu, D., Hill, A.D.: An integrated theoretical and experimental study on the effects of multiscale heterogeneities in matrix acidizing of carbonates. SPE115143. Presented at SPE Annual Technical Conference and Exhibition, Denver, Colorado, USA, 21–24 September 2008

Izgec, O., Zhu, D., Hill, A.D.: Models and methods for understanding of early acid breakthrough observed in acid core-floods of vuggy carbonates. SPE122357. Presented at SPE European Formation Damage Conference, Scheveningen, The Netherlands, 27–29 May 2009

Kalia, N., Balakotaiah, V.: Modeling and analysis of wormhole formation in reactive dissolution of carbonate rocks. Chem. Eng. Sci. **62**(4), 919–928 (2007)

Kalia, N., Balakotaian, V.: Effect of medium heterogeneities on reactive dissolution of carbonates. Chem. Eng. Sci. **64**(2), 376–390 (2009)

Kang, Q.J., Zhang, D.X., Chen, S.Y., He, X.Y.: Lattice Boltzmann simulation of chemical dissolution in porous media. Phys. Rev. E. **65**(3), 036318/1–036318/8 (2002)

Liu, X., Ormond, A., Bartko, K., Li, Y., Ortoleva, P.: A geochemical reaction-transport simulator for matrix acidizing analysis and design. J. Pet. Sci. Eng. **17**(1–2), 181–196 (1997)

Panga, M.K.R.: Multiscale transport and reaction: two case studies. Ph.D. dissertation, The University of Houston (2003)

Panga, M.K.R., Ziauddin, M., Balakotaiah, V.: Two-scale continuum model for simulation of wormholes in carbonate acidization. AIChE J. **51**(12), 3231–3248 (2005)

Schoenfelder, W., Glaser, H., Mitreiter, I., Stallmach, F.: Two-dimensional NMR relaxometry study of pore space characteristics of carbonate rocks from a Permian aquifer. J. Appl. Geophys. **65**(1), 21–29 (2008)

Tardy, P.M.J., Lecerf, B., Chrisianti, Y.: An experimentally validated wormhole model for self-diverting and conventional acids in carbonate rocks under radial flow conditions. SPE107854. Presented at SPE European Formation Damage Conference, Scheveningen, The Netherlands, 30 May–01 June 2007